ADVANCED OPTICAL MATERIALS
www.advopticalmat.de

Resonance Energy Transfer from Monolayer WS_2 to Organic Dye Molecules: Conversion of Faint Visible-Red into Bright Near-Infrared Luminescence

*Nicolas Zorn Morales, Nikolai Severin, Jürgen P. Rabe, Stefan Kirstein, Emil List-Kratochvil, and Sylke Blumstengel**

The synergetic combination of transition metal dichalcogenides (TMDCs) with organic dye molecules in functional heterostructures is promising for various optoelectronic applications. Here resonance energy transfer (RET) from a red-emitting WS_2 monolayer (1L-WS_2) to a layer of near-infrared (NIR) emitting organic dye molecules is demonstrated. It is found that the total photoluminescence (PL) yield of the heterostructures is up to a factor of eight higher as compared to the PL yield of pristine 1L-WS_2. This is attributed to the efficient conversion of the mostly non-radiative excitons in 1L-WS_2 into radiative excitons in the dye layer. A type-I energy level alignment of the 1L-WS_2/dye interface assures the emission of bright PL. From excitation density-dependent PL experiments, it is concluded that RET prevails against defect-assisted non-radiative recombination as well as Auger-type exciton-exciton annihilation in 1L-WS_2. The work paves the way for employing organic dye molecules in heterostructures with TMDCs in nanoscale light-emitting devices with improved efficiency and tunable color.

1. Introduction

Heterostructures formed between different transition metal dichalcogenides (TMDCs) or by the combination of TMDCs with other materials, like organic molecules or semiconductor quantum dots, have been studied intensively over the past years in order to tune and manipulate the absorption, luminescence, or conductivity.[1,2] For achieving the desired property, the coupling of electronic states of the constituents across the heterointerface is decisive. This has motivated many studies on exciton transfer as well as charge transfer involving the ground and excited state in TMDC-based heterostructures.[2,3,4,5–8] In particular, excited state charge transfer between the organic component and the TMDCs [5,9,10] as well as non-radiative resonance energy transfer (RET) from organic dye molecules to TMDCs [3,6,11,12] have been utilized to enhance the photosensitivity and to tune the spectral range in nanoscale photodetecting devices.[3,5,8,13] The reverse transfer of excitation energy, namely that from TMDCs to dye molecules is of special interest for the development of nanoscale electrically pumped light sources benefitting from the high PL quantum yield (up to 100%) of organic dyes as well as the wide tunability of their emission wavelength. However, two challenges are encountered here: First, a staggered type-II energy level alignment at the heterointerface is often observed that results in effective charge separation and concomitant quenching of the luminescence of both partners.[3,10,14] Second, excitation of monolayer TMDCs (1L-TMDC) is followed by fast defect-assisted non-radiative recombination as well as Auger-type exciton-exciton annihilation (EEA), the latter being already very efficient at moderate exciton densities in 2D materials.[15–17] Defects include sulfur vacancies acting as electron donors and rendering monolayer sulfides n-doped as well as more complex defects, such as antisites, transition metal vacancies, line defects, or vacancy clusters. These are reported to induce deep levels.[18] Ultrafast spectroscopy has revealed that defect-mediated carrier capture and non-radiative recombination are dominated by the Auger process.[19] To achieve RET rates that can compete with those nonradiative recombination channels in the TMDC, several requirements have to be met. A) The interactions that mediate RET, i.e., coulomb or exchange interaction, are short-ranged (typically < 5 nm) and strongly distant dependent. Therefore, the molecules must assemble in close proximity to the surface

N. Zorn Morales, E. List-Kratochvil
Department of Physics
Department of Chemistry & IRIS Adlershof
Humboldt-Universität zu Berlin
Zum Großen Windkanal 2, 12489 Berlin, Germany
N. Severin, J. P. Rabe, S. Kirstein, S. Blumstengel
Department of Physics & IRIS Adlershof
Humboldt-Universität zu Berlin
Newtonstr. 15, 12489 Berlin, Germany
E-mail: sylke.blumstengel@physik.hu-berlin.de
E. List-Kratochvil
Helmholtz-Zentrum Berlin für Materialien und Energie GmbH
Hahn-Meitner-Platz 1, 14109 Berlin, Germany

The ORCID identification number(s) for the author(s) of this article can be found under https://doi.org/10.1002/adom.202301057

DOI: 10.1002/adom.202301057

of TMDC, preferably as a homogeneous thin film. B) Sufficient spectral overlap between the donor (TMDC) PL and the acceptor (dye) absorption is needed to meet the energy resonance condition. C) To be of use in light-emitting applications, a straddling type-I interfacial energy level alignment is mandatory to avoid exciton dissociation and hence quenching of the acceptor PL. D) The intrinsic PL quantum yield of the acceptor must be as high as possible with an emission maximum in the desired wavelength range.

In this study, we demonstrate efficient RET from 1L-WS_2 as a donor to a pyronin-analog [20] near-infrared emitting dye [16] as an acceptor. The used dye Atto 725 (Atto-Tec, Germany) exhibits an outstanding photostability and a fluorescence yield of 10% which is high in comparison to other NIR dyes.[21] The strong and narrow absorption partially overlaps with the 1L-WS_2 PL but not with its absorption so that dye and TMDC can be individually optically addressed. We show that for this couple all requirements for efficient RET are met which leads to almost an order in magnitude increase of total PL intensity by simultaneous conversion of the emission energy toward NIR.

2. Results and Discussion

The RET process in 1L-WS_2/Atto hybrid structures is examined by a combination of steady-state PL and PL excitation (PLE) spectroscopy at low excitation densities as well as by time-resolved PL measurements at high pump pulse fluences. In the latter excitation regime, the RET has to compete additionally with the fast EEA in the donor. Furthermore, we compare the excited state transfer processes in hybrid structures of the dye with 1L-WS_2, bilayer (2L)-WS_2, and multilayer (ML)-WS_2. These experiments demonstrate the impact of the energy level alignment on the PL yield. The energy level alignment at the heterointerface is derived from photoelectron yield spectroscopy of the dye. Two types of WS_2 are used in the experiments, namely, large-area chemical vapor deposition (CVD)-grown 1L-WS_2 on a sapphire substrate (2D Semiconductors) and WS_2 layers manually exfoliated under nitrogen atmosphere from bulk crystals (HQ Graphene) onto mica substrates yielding 1L-WS_2, 2L-WS_2, and ML-WS_2 flakes with a lateral size of some tens of micrometers. Exfoliated monolayers on mica have a higher PL yield than CVD-grown samples (see Figure S1, Supporting Information) which agrees with the reported orders of magnitude higher defect concentration in CVD-grown monolayers.[22] Since PLE spectroscopy is performed with a commercial spectrometer (FLS980, Edinburgh Instruments) having a light beam spot size of ≈1 mm^2 and therefore requiring large-area samples, all PLE experiments are performed with CVD-grown 1L-WS_2. However, due to fast defect-assisted non-radiative recombination, the PL decay of the CVD-grown WS_2 is close to the instrument response function (IRF) of our time-correlated single photon counting set-up even at low excitation density. Therefore, all time-resolved PL measurements are performed with exfoliated WS_2 flakes in a μ-PL set-up. Also, the layer number dependent experiments are performed with exfoliated samples since this method yields single flakes comprised of 1L-, 2L-, and ML-regions.

2.1. RET at the 1L-WS_2/Atto Interface at low Excitation Density

The sample layout of the 1L-WS_2/Atto hybrid structure and the considered energy transfer process are schematically depicted in **Figure 1**a. Before evaluating the RET at low excitation density we briefly introduce the optical spectra of the individual components. In Figure 1b the PL and PLE spectra of a thin layer of Atto 725 obtained by spin-coating on mica are shown. The PLE spectrum is representative of the absorption spectrum of the dye with a characteristic absorption peak at 1.692 eV and two vibronic progressions with energy spacing of about 165 meV. The PL maximum is found at 1.640 eV. The shapes of the spectra are very similar to the respective absorption and PL spectra in aqueous solution [23], besides a small red shift by about 10 meV which is due to the different polarity of the mica surface versus water solution. Obviously, there is no modification of the absorption or emission of the dye that could be attributed to aggregation. The PL and absorbance [$-\lg(T)$, where T is the transmission] spectra of CVD-grown 1L-WS_2 are also shown in Figure 1b. The absorbance reveals the bands of the A and B excitons. The PL is dominated by recombination of neutral A excitons which spectrally overlaps with the second vibronic band of the absorption of the dye. The red emission of the TMDC can thus be converted into NIR emission of the dye, provided that the RET is sufficiently efficient. The negligible spectral overlap of the absorption of the dye's and the absorption of 1L-WS_2 provides furthermore the opportunity to utilize RET to locally read out the absorption of the TMDC as will be discussed below.

Figure 1c summarizes data collected for a hybrid structure composed of a CVD-grown 1L-WS_2 covered by the dye molecules. An AFM image of the sample is reported in Figure S2 (Supporting Information). The morphology of the molecular layer appears porous with a thickness of ≈2 nm and a total coverage of the 1L-WS_2 surface of ≈80%. The molecules are thus in sufficient proximity to the WS_2 surface which is an essential prerequisite for efficient excitation via RET. For a Förster-type transfer, mediated by dipole-dipole interaction, a rough estimate of the expected distance of the RET can be obtained from the calculation of the Förster radius R_0 from the spectral overlap integral. Assuming a PL quantum yield of CVD-grown ML-WS_2 of 1%, a mean distance $R_0 \approx 1.5$ nm is obtained (see Section S3, Supporting Information for details). This value should, however, be considered with caution, since the dipole-dipole approximation only poorly describes the present configuration where the donor and acceptor are in close proximity. Since dye and TMDC are in close contact, not only coulomb coupling but also exchange interaction is expected to contribute to the RET. The latter is, however, even more short-ranged, since it requires wave function overlap of the atomic/molecular orbitals at the heterointerface. Furthermore, in a layered structure, the energy transfer rate depends on the density and layer thickness of the acceptor dye molecules.[24]

The absorbance [$-\lg(T)$] of the 1L-WS_2/Atto hybrid structure is shown in the lower panel of Figure 1c. It is a linear superposition of the absorption features of 1L-WS_2 and that of the dye. It should be noted that $T = 1 - A - R$ with A being the absorption and R the reflectivity. For thin layers ($d \ll$ wavelength of light) on transparent substrates the R and A spectra have the same shape.[25] Transfer matrix method simulations (see Section

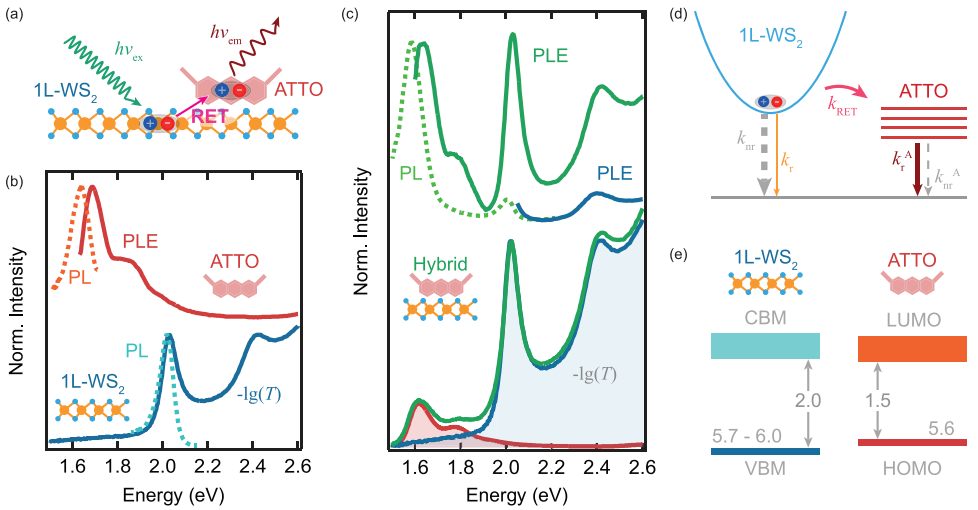

Figure 1. a) Design of the 1L-WS_2 /Atto hybrid structure and schematic depiction of the energy transfer process. b) Optical spectra of the individual components: PL (orange dashed) and PLE (red solid) spectra of an Atto725 dye layer. The PL of the dye is excited at 1.76 eV and the PLE recorded setting the detection energy to the low energy side of the PL spectrum at 1.6 eV. PL (light blue dashed) and absorbance [– lg(*T*)] (dark blue solid) spectra of CVD-grown 1L-WS_2 on sapphire. The PL is excited non-resonantly at 2.82 eV. c) Optical spectra of the 1L-WS_2/Atto hybrid structure using a CVD-grown monolayer: Lower panel: Absorbance of the hybrid structure (dark green solid). The spectrum is a superposition of the absorbance of 1L-WS_2 (blue shade) and of the dye (red shade). The latter is obtained by normalizing the PLE spectrum of the dye on mica to the respective absorption maximum in the hybrid structure and shifting the spectrum by +60 meV. The different polarities of the substrate account for this spectral shift. Upper panel: PLE spectra of the hybrid structure recorded at the low-energy sides of the 1L-WS_2 emission at 1.97 eV (dark blue solid) and the dye at 1.56 eV (dark green solid). The PL spectrum of the hybrid structure (light green dashed) is obtained by exciting the sample at 2.82 eV. All spectra are measured at room temperature at very low excitation power (<0.5 W cm^{-2}). d) Scheme of the RET process at low excitation density: After generation of A excitons in 1L-WS_2 the RET rate (k_{RET}) competes with the radiative (k_r) and nonradiative (k_{nr}) deactivation rates. In the CVD-grown monolayer, the latter is governed by defect-assisted nonradiative recombination. e) Energy level alignment at the 1L-WS_2/Atto hybrid structure. All energy values are given in eV and rounded to 50 meV.

S4 and Figure S3, Supporting Information for details) yield that the ratio of photons absorbed in the dye layer A_{dye} at 1.615 eV and those absorbed in the 1L-WS_2 A_{1L} at 2.022 eV is about one third: $\frac{A_{1L}(2.022\ \text{eV})}{A_{dye}(1.615\ \text{eV})} = 1/3$. The lower panel of Figure 1c summarizes PL and PLE spectra of the 1L-WS_2/Atto hybrid structure. The PLE spectrum recorded at the emission energy of 1L-WS_2 shows the absorption of the B exciton. Due to the small Stokes shift, only the high energy side of the A excitonic resonance is resolved. In contrast, the PLE spectrum recorded at the emission energy of the dye reproduces the full absorption spectrum of the 1L-WS_2 including A and B excitonic transitions and also the absorption features of the dye. The fact that PL of the dye is clearly generated when the hybrid structure is excited in spectral regions where the molecules do not absorb provides direct evidence that the excitons created by absorption in 1L-WS_2 are converted via RET into excitons in the dye layer. Those excitons then recombine radiatively with their given quantum efficiency in the heterostructure as shown schematically in Figure 1d. It should be noted that the reabsorption of photons emitted by 1L-WS_2 by the dye is negligible due to the low absorbance and PL quantum yield of the TMDC monolayer. The PLE spectrum provides thus an estimate of the RET efficiency η_{RET}. The ratio of the PLE intensity ratio at the absorption maximum of the dye (at 1.615 eV) and the A excitonic resonance (at 2.022 eV) of the 1L-WS_2 is about unity: $\frac{I_{PLE}(2.022\ \text{eV})}{I_{PLE}(1.615\ \text{eV})} = 1$ (upper panel in Figure 1c). In general, the PL intensity recorded at the emission maximum of the dye at 1.56 eV excited at an energy $\hbar\omega$ results from direct absorption of the dye and from the excitation of the 1L-WS_2 that is transferred to the dye. Thus, the total PLE intensity can be written as:

$$I_{PLE}(\hbar\omega) \propto \left(A_{dye}(\hbar\omega) + \eta_{RET} \times A_{1L}(\hbar\omega)\right)\eta_{dye} \quad (1)$$

η_{dye} is the PL quantum efficiency of the dye in the hybrid structure. The absorbance of the dye is nearly zero at the A excitonic transition of 1L-WS_2 at $\hbar\omega = 2.022$ eV and, vice versa, the absorbance of 1L-WS_2 vanishes at the peak absorbance of the dye at $\hbar\omega = 1.615$ eV. This yields the simple expression for the PLE intensity ratios at the two energies:

$$\frac{I_{PLE}(2.022\ \text{eV})}{I_{PLE}(1.615\ \text{eV})} = \eta_{RET} \times \frac{A_{1L}(2.022\ \text{eV})}{A_{dye}(1.615\ \text{eV})} \quad (2)$$

and hence, in the present hybrid structure, a RET efficiency of $\eta_{RET} \approx 0.33$ is obtained.

The PL of the hybrid structure excited at 2.82 eV is dominated by the emission of the dye (Figure 1c). The emission of 1L-WS_2 is reduced in the hybrid structure as compared to the pristine monolayer by the fraction of excitons that is transferred via RET to the dye. The total PL output of the present hybrid structure I_{hyb} is enhanced as compared to I_{ref} of the pristine CVD-grown 1L-WS_2 by a factor $f = \frac{I_{hyb}}{I_{ref}} \approx 8$ due to RET. The factor is calculated from the PL spectra in Figure 1 recorded with an excitation energy where the dye is transparent. I_{hyb} is obtained by integrating the PL of the hybrid structure over the whole spectral range

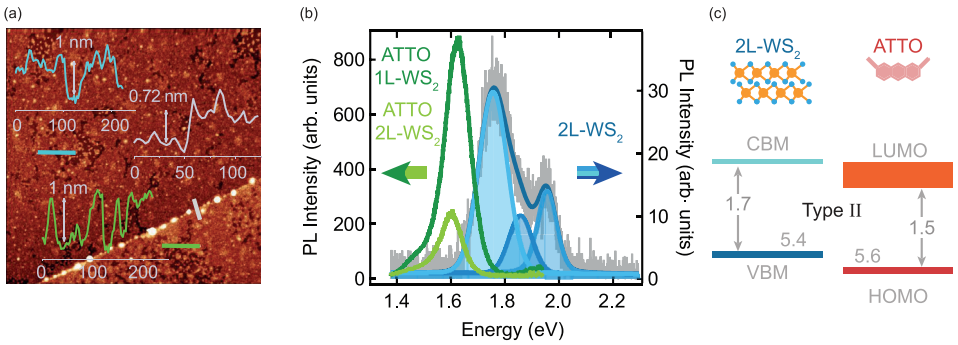

Figure 2. a) AFM image of spin-coated Atto 725 on an exfoliated WS_2 flake comprising 1L and 2L regions. The height profiles are recorded along the lines of the same color: blue: on 1L-WS_2, green on 2L-WS_2, and white: across the 1L-2L step. All values are given in nm. b) PL spectra of 1L-WS_2/Atto (dark green) and 2L-WS_2/Atto (light green). The excitation photon energy is 1.94 eV, i.e., smaller than the absorption edge due to the direct bandgap of WS_2 and therefore only PL of the dye is generated. For comparison, a magnified PL spectrum of a bare 2L-WS_2 (grey) excited at 1.76 eV is shown as well. The spectrum is fitted with three pseudo-Voigt profiles (blue) corresponding to the emission of the A exciton (1.955 eV), defect emission (1.850 eV), and PL from the indirect optical gap (1.755 eV). c) Energy level alignment at the 2L-WS_2/Atto interfaces. For details see main text. All values are given in eV and rounded to 50 meV.

while I_{ref} is the integrated PL of the pristine 1L-WS_2. The substantial increase is explained by the fact that the RET rate $k_{RET} \approx 0.5(k_r + k_{nr}) \approx 0.5 \cdot k_{nr}$ can not only compete with the radiative k_r, but also with the much faster non-radiative recombination rate k_{nr} in 1L-WS_2 which is the dominating deactivation channel of excitons in CVD-grown TMDC monolayers [16]. A large fraction of otherwise nonradiatively recombining TMDC excitons is thus rescued via RET and converted into radiative excitons of the dye fostered by its high PL quantum efficiency.

At this point, it should be emphasized that efficient RET is a necessary but not a sufficient condition to achieve such PL enhancement.[14] As pointed out above, another prerequisite is that the intrinsically high PL yield of the dye is maintained when in direct contact with the 1L-WS_2 and this requires a straddling energy level alignment of type-I at the heterointerface.[14] Indeed, photoelectron yield spectroscopy of the dye implies such type-I energy level alignment as shown in Figure 1e where the energy offsets between the occupied and unoccupied levels have a different sign. The position of the dye's highest occupied molecular orbital (HOMO) is obtained from photoelectron yield spectroscopy (see Section S5, Supporting Information), while the energy of valence band maximum (VBM) at the K-point (5.7–6 eV) is taken from literature.[26,27] The positions of the dye's lowest unoccupied molecular orbital (LUMO) and of the conduction band maximum (CBM) of 1L-WS_2 are obtained by adding the respective electronic bandgap energy E_g to the HOMO and VBM, respectively. The gap energies given in Figure 1e correspond to the optical bandgaps E_{opt} derived from the absorption spectra of the dye and 1L-WS_2. The contribution of exciton binding energy E_B to $E_g = E_{opt} + E_B$ is indicated by the shaded areas in Figure 1e. E_B is ≈200–300 meV for the 1L-WS_2.[28] The difference between the optical and the HOMO-LUMO gap is not known for the present dye. It is typically a few hundreds of meV for organic molecules. Despite the uncertainties of the positions of the unoccupied level, it can be safely concluded that the energy level alignment at the hybrid interface provides no driving force for exciton dissociation and excited state (single) charge transfer between the dye and 1L-WS_2. As a consequence, the high PL yield is maintained in the 1L-WS_2/Atto hybrid structure. It should be noted that simultaneous electron–hole transfer from 1L-WS_2 to Atto via a Dexter-type transfer is possible and may provide a channel for RET. In hybrid structures with 2L-WS_2 or ML-WS_2, a very different scenario is observed. This is discussed in the next section.

2.2. Excited State Charge Versus Energy Transfer as Function of the WS_2 Layer Number

The exfoliation process on mica results in WS_2 flakes comprised of 1L, 2L, and ML regions. Via μ-PL measurements, excited state transfer processes are evaluated as a function of the TMDC layer number. **Figure 2**a shows an AFM image of a WS_2 flake covered by the dye. The flake is comprised of 1L- and 2L-WS_2 as evidenced by the height profile taken along the step edge and by PL measurements showing the typical PL signal of 1L- and 2L-WS_2 (see below). The morphology of the molecular layer does not differ on 1L- and 2L-WS_2. In both regions, the molecular coverage is ≈ 80% and the layer height ≈ 1 nm. As the excitation laser spot diameter is 0.9 µm, inhomogeneities of the molecular layer are averaged out. Figure 2b compares the PL spectra of the dye on 1L-WS_2 and 2L-WS_2. Further, PL line scans were taken across 1L- and 2L regions of the WS_2 flake as well as along 1L- and ML regions of a different flake are reported in Figure S6 (Supporting Information). Importantly, the excitation energy is at 1.94 eV, i.e., below the absorption edge due to the direct bandgap of WS_2 so that the dye molecules are selectively excited and indirect excitation via energy transfer is ruled out. A strong decrease in the PL of the dye is observed on 2L-WS_2. On ML-WS_2, the quenching is even stronger and no PL signal of the dye is detectable any longer. To reveal the mechanism of the strong PL quenching of the dye, a PL spectrum of the 2L-WS_2 before the deposition of the molecules is depicted for comparison in Figure 2b. It should be noted that the PL spectrum of the 1L-WS_2 region shows the typical emission of the A exciton (like in Figure 1c) confirming the monolayer thickness of the region. The 2L-WS_2 spectrum can be deconvoluted into contributions of the A exciton (peak at 1.955 eV), defect emission (peak at 1.850 eV) (which is very weakly observable also in 1L-WS_2), and emission at the

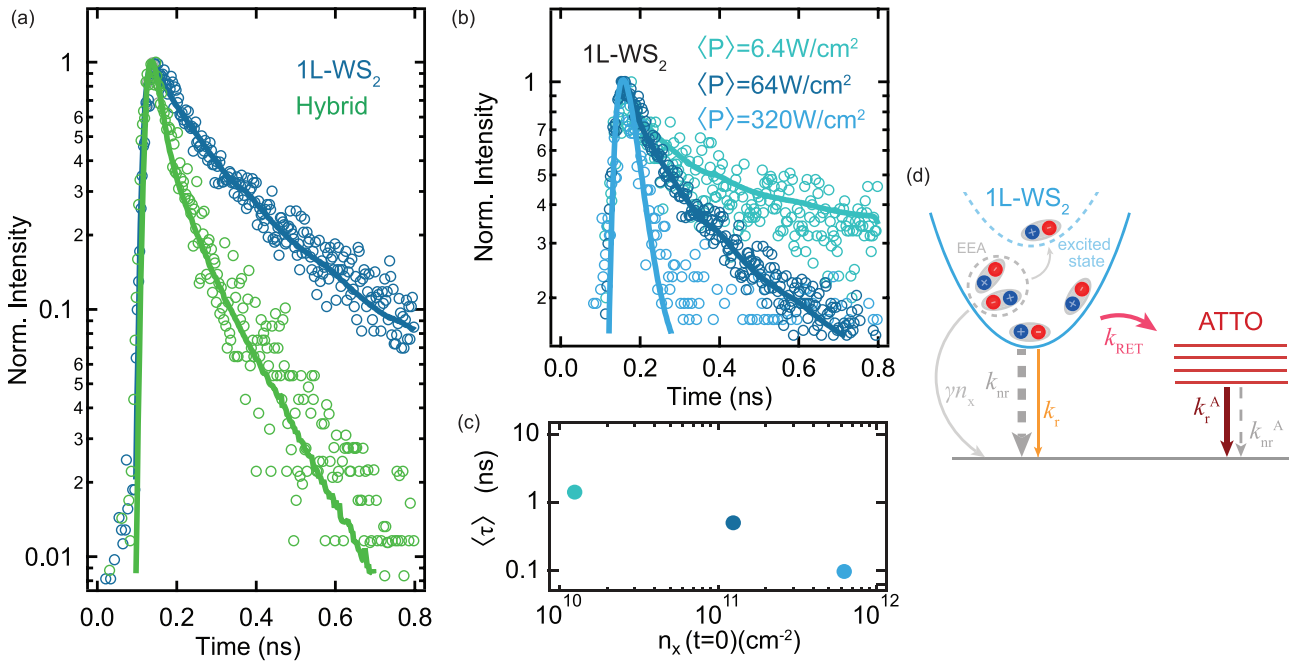

Figure 3. a) PL transients of pristine 1L-WS_2 (blue dots) and of the 1L-WS_2/Atto hybrid structure (green dots) The excitation energy is 2.82 eV and the PL is detected at the emission maximum of the 1L-WS_2 A-exciton at 2.02 eV. The IRF is shown in Figure S1b (Supporting Information). The excitation power is 64 W/cm^2. This translates into an initial exciton density of n_X ($t = 0$) = 1.25 × $10^{11}$$cm^{-2}$. b) PL transients of pristine 1L-WS_2 at varied pump pulse fluences [7]. The solid lines in (a) and (b) fit the decay curves obtained by convoluting a bi-exponential decay law with the IRF. c) Dependence of the mean PL decay time $\langle\tau\rangle$ (see main text for definition) pristine 1L-WS_2 on $n_X(t = 0)$. d) Scheme of the competing processes in the hybrid structure at high pump pulse fluences. RET competes with radiative, defect-assisted non-radiative as well as Auger-type EEA in the 1L-WS_2 donor. The rate γn_X of the latter depends on the exciton density n_X.

indirect optical gap energy (peak at 1.755 eV) due to a transition from conduction band minimum (CBM) at midpoint between K and Γ points and valence band maximum (VBM) at the Γ point.[29] Since the PL of the dye is emitted at energies below the indirect optical gap of 2L-WS_2, back energy transfer from the dye to the TMDC via a Dexter-type transfer mechanism is very unlikely and cannot explain the strong quenching of the molecule's PL.

The explanation of the strong PL quenching is found in Figure 2c which shows the energy level alignment at the 2L-WS_2/Atto hybrid interfaces. The VBM of 2L-WS_2 moves in momentum space to the Γ-point and the energy shifts upward above the dye's HOMO to ≈ 5.4 eV.[26] The LUMO position of 2L-WS_2 is estimated by adding the optical bandgap energy to the VBM. Due to the increased screening, the E_B in 2L-WS_2 is reduced and therefore its contribution to E_g neglected.[30] The resultant energy level alignment is thus of type-II. Hence, excitation of the dye may be followed by hole transfer from its HOMO to the valence band of the TMDC. As a result of the dissociation of the dye's excitons at the hybrid interface, its PL yield is strongly reduced. Such a type-II energy level alignment is obviously detrimental for applications of TMDC/dye heterostructures in light-emitting devices where the dye serves as the emitter material. The introduction of a spacer layer between TMDC and dye would help to avoid charge separation and concomitant quenching of the PL. However, since RET is very short-ranged, a spacer layer would also reduce the RET rate and efficiency. Therefore, the proper selection of the acceptor dye molecule is crucial.

2.3. RET at the 1L-WS_2/Atto Interface at High Excitation Density

The RET efficiency η_{RET} and the RET time constant τ_{RET} can be directly obtained from time-resolved PL measurements. In that case, the excitation intensity from the pulsed laser excitation easily reaches values where the Auger-type EEA process becomes important, as will be seen in the following. The high-density pulse excitation measurements are performed with individual exfoliated 1L-WS_2 flakes before and after coverage with the molecules. This procedure proofed essential since the PL quantum yield and thus the PL decay time varies from flake to flake due to possible strain and/or a different concentration of defect sites introduced by the exfoliation process (see Figure S1, Supporting Information). The data presented in **Figure 3** are obtained with one of the brightest flakes which has a PL quantum yield about twenty times larger than the CVD-grown monolayer used for the steady state PL experiments. The PL decay of pristine 1L-WS_2 (Figure 3a) is non-exponential and becomes faster with increasing laser pump fluence (Figure 3b,c) which is indicative of an additional decay channel of 1L-WS_2 A excitons due to Auger-type EEA. EEA in monolayer TMDCs under pulsed excitation at similar initial exciton densities of n_X ($t = 0$) = 10^{11} − $10^{12}$$cm^{-2}$ is repeatedly reported in literature.[15,17,31] In comparison, the above presented steady state PL and PLE measurements are performed at an excitation rate of ≈ 7 × $10^{16}$$cm^{-2}s^{-1}$ which corresponds to a steady state exciton density of only n_X < ≈7 × $10^7$$cm^{-2}$ assuming an A exciton lifetime of about ≈ 1 ns [17] (see Section S7, Supporting Information) when EEA is ineffective. The PL decay in the

1L-WS_2/Atto hybrid structure is also non-exponential and, most importantly, noticeably shortened (Figure 3a) which indicates that RET due to a nonradiative Förster- or Dexter-type process must be efficient also at high pump fluences. The PL transients are fitted with a bi-exponential decay law convoluted with the IRF to obtain a mean lifetime defined by $\langle\tau\rangle = \int t \times I(t)\mathrm{d}t / \int I(t)\mathrm{d}t$. For pristine 1L-$WS_2$ the mean PL decay time is $\langle\tau_{1L}\rangle = 380$ ps. RET to the dye molecules reduces the lifetime of the A exciton in the hybrid structure to $\langle\tau_h\rangle = 110$ ps. This yields an estimate of the RET time constant $\tau_{RET} \lesssim 150$ ps. The inequality reflects that the PL decay in the hybrid structure is already close to the IRF and therefore only an upper estimate can be given. The RET rate exceeds thus all deactivation rates in 1L-WS_2 at least by a factor of 2.5. A lower bound for the efficiency of RET is given by $\eta_{RET} = (I_0 - I_h)/I_0$, where I_0 and I_h are the 1L-WS_2 PL yields of the pristine monolayer and in the hybrid structure, respectively, obtained by integrating the normalized PL transients after deconvolution with the IRF. Under the present excitation conditions [n_X $(t = 0) = 1.25 \times 10^{11}\mathrm{cm}^{-2}$], $\eta_{RET} \approx 0.8$ is obtained which is quite surprising since it is even higher than that obtained by the steady state PLE at low excitation density with the CVD-grown 1L-WS_2 as donor. Actually, the opposite trend is expected since at high pump fluences, RET has not only to compete with radiative and defect-assisted nonradiative exciton recombination in 1L-WS_2 but also with Auger-type EEA as shown in Figure 3c, and therefore, η_{RET} should become smaller. The result can be understood by comparing the different rate constants: While the radiative recombination rate k_r of 1L-WS_2 is an intrinsic material parameter, the nonradiative recombination rate k_{nr} depends strongly on the defect concentration and thus on the fabrication conditions. As pointed out above, the CVD-grown 1L-WS_2 has about one order of magnitude smaller PL quantum yield η_{WS_2} than exfoliated samples. Taking into consideration $\eta_{WS_2} \ll 1$ suggests that the defect-assisted nonradiative decay rate k_{nr} in the CVD-grown monolayer is about one order of magnitude faster than in exfoliated monolayers. As a result, k_{nr} of the CVD-1L-WS_2 exceeds the RET rate ($\eta_{RET} < 0.5$), and it is apparently also larger than the EEA rate at the exciton densities created with the pulsed excitation because in the high-quality exfoliated monolayer, the RET rate k_{RET} prevails over all deactivation channels in 1L-WS_2 including Auger-type EEA ($\eta_{RET} > 0.5$).

Finally, we can provide an estimate on the enhancement factor $f = \frac{I_{hyb}}{I_{ref}}$ obtained for exfoliated 1L-WS_2 as donor. The PL intensity of pristine 1L-WS_2 is $I_{ref} = I_0\, A_{1L}\eta_{1L}$ with I_0 being the excitation intensity. Choosing an excitation energy where only 1L-WS_2 absorbs and the dye is only excited via RET yields the total PL intensity of the hybrid structure $I_{hyb} = (1 - \eta_{RET})\, I_{ref} + \eta_{RET} I_0 A_{WS_2}\eta_{dye}$. Consequently, the enhancement factor becomes $f = 1 + \eta_{RET}(\frac{\eta_{dye}}{\eta_{1L}} - 1)$. It is obvious that $f > 1$ is only achieved when $\eta_{dye} > \eta_{1L}$. For the hybrid structure with the CVD-grown 1L-WS_2 we have found $f \approx 8$. Taking the literature value $\eta_{dye} \approx 0.1$ yields an estimate of $\eta_{1L} \approx 0.5\%$ agreeing with reported values.[16] The best of our exfoliated 1L-WS_2 has a PL yield about 20 times higher than that of the CVD-grown monolayer at sufficiently low excitation density. This implies that $\eta_{1L} \approx \eta_{dye}$ and therefore, the PL enhancement factor f is unity. However, this is true only as long as EEA is negligible. Increasing the excitation intensity, EEA sets in, and the PL yield of 1L-WS_2 drops. For the present monolayer, we find that increasing $n_X(t = 0)$ from 1.25×10^{10} to $1.25 \times 10^{11}\mathrm{cm}^{-2}$ lowers the PL yield by about a factor of 3. The value is obtained by integrating the respective normalized PL transients after deconvolution with the IRF (Figure 3b) and calculating the ratio. Consequently $\eta_{1L} \leq 0.33\eta_{dye}$ and $f \geq 2.5$. The inequality arises since at the lowest studied n_X $(t = 0) = 1.25 \times 10^{10}\mathrm{cm}^{-2}$ the occurrence of EEA cannot be entirely ruled out. At the highest studied excitation density n_X $(t = 0) = 1.25 \times 10^{12}\mathrm{cm}^{-2}$, the PL transient of the pristine 1L-WS_2 approaches the IRF. Therefore, the RET efficiency and consequently the enhancement factor f cannot be estimated but the number given sets a lower limit.

3. Conclusion

To summarize, RET from a 1L-WS_2 to an adjacent dye layer with an efficiency of up to 80% has been revealed. As a result, the emission color is converted from visible red to NIR, and the total PL yield of the hybrid structure is enhanced by up to a factor of eight as compared to the pristine monolayer. Our experiments show that RET can compete not only with defect-assisted nonradiative recombination but also with Auger-type EEA at high pump fluences. As a result, excitons that would undergo nonradiative recombination in the TMDC are converted into bright excitons of the dye layer. Via RET the notoriously low PL quantum yield of TMDCs in particular at high pump fluences can thus be overcome. The prerequisite is that the acceptor molecules maintain their intrinsically high PL quantum yield in the hybrid structures and this requires a type-I interfacial energy level alignment. Such TMDC/dye hybrid structures supporting RET have potential in nanoscale light sources where the TMDC is electrically driven while light with the desired emission color is emitted efficiently from the dye. The presented results show that even a rather small spectral overlap can lead to efficient RET which is due to the very large transition dipole moment of TMDC excitons and an intimate contact of donor and acceptor. The choice of suitable acceptor molecules and with that the tuning range of the emission color is thus large. An in-depth discussion of the underlying mechanism of the RET will be a topic of future work. It is expected that both Förster- as well as Dexter-type transfer are contributing to RET. As Dexter-type transfer requires wavefunction overlap between donor and acceptor, it can be switched off by introducing an interlayer, for example, hBN, between TMDC and dye. This would provide the opportunity to study RET by the Förster mechanism individually. The different dimensionality of the excitons in the two materials, namely delocalized Wannier-Mott excitons in the 2D plane of the TMDC and Frenkel excitons localized at the molecule (or delocalized in an aggregate comprising several molecules) is expected to result in peculiarities which are not captured by the classical Förster theory developed for molecular donor-acceptor systems as shown in theoretical works.[12,32] This calls for further in-depth experimental studies. Both Förster- and Dexter-transfer are short-ranged and this offers yet another application of RET. The process can be exploited to study optical transitions in the TMDC with unprecedented spatial resolution. As shown in Figure 1c, due to the negligible overlap of the dye and 1L-WS_2 absorption, the unobscured full PLE spectrum of the TMDC can be measured via the detection of the dye's emission. With sufficient dilution, a single dye

molecule or a small molecular cluster can thus serve as a local probe to read out the optical properties of the TMDC within the characteristic RET radius, i.e., with a spatial resolution of a few nm.

4. Experimental Section

Photoluminescence Spectroscopy: Photoluminescence (PL) and PL excitation (PLE) experiments were performed with a commercially available FLS980 spectrometer (Edinburgh Instruments Ltd) using a Xenon arc lamp as excitation source. The spot size in this setup was ≈ 1 mm^2 with an excitation power of < 0.5 W cm^{-2}. μ-PL measurements have been performed with a home-built setup using a cw laser diode emitting at 2.82 eV (Picoquant) as excitation source. The laser spot diameter was 1 μm.

The PL line scan shown in Figure S6 (Supporting Information) was acquired with a Raman instrument (XploRA, Horiba Ltd.) using a 638 nm laser for excitation with 2.4 μW excitation power on the sample surface. The laser spot diameter was 0.9 μm.

Time-resolved PL was recorded with the same μ-PL setup employing the time-correlated single photon counting (TCSPC) technique. A mode-locked frequency-doubled fs-Ti:sapphire laser (76 MHz) served as excitation source. The time-resolved experiments had been performed at an excitation energy of 2.82 eV at varied average excitation power. The overall time resolution was 30 ps.

Photoelectron Yield Spectroscopy (PYS): PYS had been performed using a commercially available AC-2 Spectrometer from Riken Keiki. An Indium Tin Oxide (ITO) substrate was used to avoid charging of the sample. The substrate was cleaned by rinsing subsequently in Acetone and Isopropanol followed by an oxygen plasma treatment for 5 min. PYS was measured before and after coating the substrate with the dye. The dye layer was deposited by spin coating from chloroform solution.

All spectroscopic measurements were performed in an ambient atmosphere.

Supporting Information

Supporting Information is available from the Wiley Online Library or from the author.

Acknowledgements

The authors gratefully acknowledge financial support by the Deutsche Forschungsgemeinschaft through CRC 951 (Project number 182087777). Furthermore, support by the Joint Lab GEN_FAB and the HySprint Innovation Lab at Helmholtz-Zentrum Berlin is acknowledged.

Open access funding enabled and organized by Projekt DEAL.

Conflict of Interest

The authors declare no conflict of interest.

Data Availability Statement

The data that support the findings of this study are available from the corresponding author upon reasonable request.

Keywords

2D semiconductors, exciton-exciton annihilation, NIR dye, resonance energy transfer, transition metal dichalcogenides

Received: May 5, 2023
Revised: June 27, 2023
Published online: July 21, 2023

[1] a) D. Jariwala, T. J. Marks, M. C. Hersam, *Nat. Mater.* **2017**, *16*, 170; b) Y. Liu, N. O. Weiss, X. Duan, H.-C. Cheng, Y. Huang, X. Duan, *Nat. Rev. Mater.* **2016**, *1*, 16042; c) M. Gobbi, E. Orgiu, P. Samorí, *Adv. Mater.* **2018**, *30*, 1706103.

[2] a) A. M. Steiner, F. Lissel, A. Fery, J. Lauth, M. Scheele, *Angew. Chem., Int. Ed.* **2021**, *60*, 1152; b) X. Xu, Z. Lou, S. Cheng, P. C. Y. Chow, N. Koch, H.-M. Cheng, *Chem* **2021**, *7*, 2989.

[3] C.-H. Cheng, Z. Li, A. Hambarde, P. B. Deotare, *ACS Appl. Mater. Interfaces* **2018**, *10*, 39336.

[4] a) Z. Hu, X. Liu, P. L. Hernández-Martínez, S. Zhang, P. Gu, W. Du, W. Xu, H. V. Demir, H. Liu, Q. Xiong, *InfoMat* **2022**, *4*, e12290; b) C. Jin, E. Y. Ma, O. Karni, E. C. Regan, F. Wang, T. F. Heinz, *Nat. Nanotechnol.* **2018**, *13*, 994; c) S. Park, H. Wang, T. Schultz, D. Shin, R. Ovsyannikov, M. Zacharias, D. Maksimov, M. Meissner, Y. Hasegawa, T. Yamaguchi, *Adv. Mater.* **2021**, *33*, 2008677; d) N. Taghipour, P. L. Hernandez Martinez, A. Ozden, M. Olutas, D. Dede, K. Gungor, O. Erdem, N. K. Perkgoz, H. V. Demir, *ACS Nano* **2018**, *12*, 8547; e) A. O. A. Tanoh, N. Gauriot, G. Delport, J. Xiao, R. Pandya, J. Sung, J. Allardice, Z. Li, C. A. Williams, A. Baldwin, S. D. Stranks, A. Rao, *ACS Nano* **2020**, *14*, 15374.

[5] N. Mutz, S. Park, T. Schultz, S. Sadofev, S. Dalgleish, L. Reissig, N. Koch, E. J. W. List-Kratochvil, S. Blumstengel, *J. Phys. Chem. C* **2020**, *124*, 2837.

[6] S. Park, N. Mutz, S. A. Kovalenko, T. Schultz, D. Shin, A. Aljarb, L. J. Li, V. Tung, P. Amsalem, E. J. List-Kratochvil, *Adv. Sci.* **2021**, *8*, 2100215.

[7] F. Prins, A. J. Goodman, W. A. Tisdale, *Nano Lett.* **2014**, *14*, 6087.

[8] D. B. Sulas-Kern, E. M. Miller, J. L. Blackburn, *Energy Environ. Sci.* **2020**, *13*, 2684.

[9] a) K. Greulich, A. Belser, S. Bölke, P. Grüninger, R. Karstens, M. S. Sättele, R. Ovsyannikov, E. Giangrisostomi, T. V. Basova, D. Klyamer, T. Chassé, H. Peisert, *J. Phys. Chem. C* **2020**, *124*, 16990; b) T. R. Kafle, B. Kattel, P. Yao, P. Zereshki, H. Zhao, W.-L. Chan, *J. Am. Chem. Soc.* **2019**, *141*, 11328; c) E. P. Nguyen, B. J. Carey, C. J. Harrison, P. Atkin, K. J. Berean, E. D. Gaspera, J. Z. Ou, R. B. Kaner, K. Kalantar-Zadeh, T. Daeneke, *Nanoscale* **2016**, *8*, 16276.

[10] T. A. Shastry, I. Balla, H. Bergeron, S. H. Amsterdam, T. J. Marks, M. C. Hersam, *ACS Nano* **2016**, *10*, 10573.

[11] J. Gu, X. Liu, E.-c. Lin, Y.-H. Lee, S. R. Forrest, V. M. Menon, *ACS Photonics* **2018**, *5*, 100.

[12] M. Katzer, S. Kovalchuk, K. Greben, K. I. Bolotin, M. Selig, A. Knorr, *Phys. Rev. B* **2023**, *107*, 035304.

[13] H. Li, Z. Dong, Y. Zhang, L. Li, Z. Wang, C. Wang, K. Zhang, H. Zhang, *2D Mater.* **2021**, *8*, 012001.

[14] R. Schlesinger, F. Bianchi, S. Blumstengel, C. Christodoulou, R. Ovsyannikov, B. Kobin, K. Moudgil, S. Barlow, S. Hecht, S. R. Marder, F. Henneberger, N. Koch, *Nat. Commun.* **2015**, *6*, 6754.

[15] Y. Lee, T. T. Tran, Y. Kim, S. Roy, T. Taniguchi, K. Watanabe, J. I. Jang, J. Kim, *ACS Photonics* **2022**, *9*, 873.

[16] S. Roy, A. S. Sharbirin, Y. Lee, W. B. Kim, T. S. Kim, K. Cho, K. Kang, H. S. Jung, J. Kim, *Nanomaterials* **2020**, *10*, 1032.

[17] L. Yuan, L. Huang, *Nanoscale* **2015**, *7*, 7402.

[18] a) Z. Wu, W. Zhao, J. Jiang, T. Zheng, Y. You, J. Lu, Z. Ni, *J. Phys. Chem. C* **2017**, *121*, 12294; b) H. Y. Jeong, Y. Jin, S. J. Yun, J. Zhao, J. Baik, D. H. Keum, H. S. Lee, Y. H. Lee, *Adv. Mater.* **2017**, *29*, 1605043.

[19] a) H. Wang, C. Zhang, F. Rana, *Nano Lett.* **2015**, *15*, 339; b) Y. Li, J. Shi, H. Chen, R. Wang, Y. Mi, C. Zhang, W. Du, S. Zhang, Z. Liu, Q.

Zhang, X. Qiu, H. Xu, W. Liu, Y. Liu, X. Liu, *Nanoscale* **2018**, *10*, 17585; c) H. Wang, J. H. Strait, C. Zhang, W. Chan, C. Manolatou, S. Tiwari, F. Rana, *Phys. Rev. B* **2015**, *91*, 165411; d) H. Wang, C. Zhang, F. Rana, *Nano Lett.* **2015**, *15*, 8204; e) M. Zhou, W. Wang, J. Lu, Z. Ni, *Nano Res.* **2021**, *14*, 29.

[20] T. Pastierik, P. Šebej, J. Medalová, P. Štacko, P. Klán, *J. Org. Chem.* **2014**, *79*, 3374.

[21] K. Rurack, M. Spieles, *Anal. Chem.* **2011**, *83*, 1232.

[22] L. Yuan, T. Wang, T. Zhu, M. Zhou, L. Huang, *J. Phys. Chem. Lett.* **2017**, *8*, 3371.

[23] https://www.atto-tec.com/ATTO-725.html?language=en (accessed: July 2023).

[24] B. Richter, S. Kirstein, *J. Chem. Phys.* **1999**, *111*, 5191.

[25] J. D. E. McIntyre, D. E. Aspnes, *Surf. Sci.* **1971**, *24*, 417.

[26] K. Keyshar, M. Berg, X. Zhang, R. Vajtai, G. Gupta, C. K. Chan, T. E. Beechem, P. M. Ajayan, A. D. Mohite, T. Ohta, *ACS Nano* **2017**, *11*, 8223.

[27] J. Ma, P. Amsalem, T. Schultz, D. Shin, X. Xu, N. Koch, *Adv. Electron. Mater.* **2021**, *7*, 2100425.

[28] a) A. Chernikov, A. M. van der Zande, H. M. Hill, A. F. Rigosi, A. Velauthapillai, J. Hone, T. F. Heinz, *Phys. Rev. Lett.* **2015**, *115*, 126802; b) W.-T. Hsu, J. Quan, C.-Y. Wang, L.-S. Lu, M. Campbell, W.-H. Chang, L.-J. Li, X. Li, C.-K. Shih, *2D Mater.* **2019**, *6*, 025028.

[29] W. Zhao, Z. Ghorannevis, L. Chu, M. Toh, C. Kloc, P.-H. Tan, G. Eda, *ACS Nano* **2013**, *7*, 791.

[30] Y. Liu, X. Hu, T. Wang, D. Liu, *ACS Nano* **2019**, *13*, 14416.

[31] a) S. Mouri, Y. Miyauchi, M. Toh, W. Zhao, G. Eda, K. Matsuda, *Phys. Rev. B* **2014**, *90*, 155449; b) S. Z. Uddin, E. Rabani, A. Javey, *Nano Lett.* **2021**, *21*, 424; c) Y. Hoshi, T. Kuroda, M. Okada, R. Moriya, S. Masubuchi, K. Watanabe, T. Taniguchi, R. Kitaura, T. Machida, *Phys. Rev. B* **2017**, *95*, 241403.

[32] D. Basko, G. C. La Rocca, F. Bassani, V. M. Agranovich, *Eur Phys J B* **1999**, *8*, 353.

[33] J. R. Lakowicz, *Principles of Fluorescence Spectroscopy*, 3rd ed., Springer, Berlin, Germany **2006**.

[34] G.-H. Jung, S. Yoo, Q. H. Park, *Nanophotonics* **2019**, *8*, 263.

[35] G. A. Ermolaev, D. I. Yakubovsky, Y. V. Stebunov, A. V. Arsenin, V. S. Volkov, *J. Vac. Sci. Technol., B* **2019**, *38*, 014002.